JOURNAL OF GUIDANCE, CONTROL, AND DYNAMICS
Vol. 21, No. 1, January–February 1998

Guidance of a Roll-Only Camera for Ground Observation in Wind

P. G. Thomasson*
Cranfield University, Cranfield MK43 0AL, England, United Kingdom

How a nose-mounted imaging sensor with a single-motion axis in roll can be used for ground observation is demonstrated. It is shown that point, line, and area observation are all possible in the presence of wind. Continuous point observation is possible by the use of an orbital trajectory in conjunction with a lookdown angle of 90 deg. For other lookdown angles the trajectories are spirals. Algorithms are derived for aircraft guidance including the cases of arbitrary lookdown angles and stationary or moving ground points, and the effects are illustrated using a six-degree-of-freedom simulation model. The effects of aircraft attitude, wind estimation, and height errors are discussed.

Nomenclature

C = orbit circumference
c = C/H
E = distance east
e = E/H
g = acceleration due to gravity
H = altitude
K_ψ = heading control gain
N = distance north
n = N/H
n_{acc} = load factor
R = ground range from target to aircraft
R_0 = perifocus range
r = R/H
T = orbital period
$\boldsymbol{u}$ = inertial velocity vector
u_r = airspeed
$\boldsymbol{u}_r$ = airspeed vector
$\boldsymbol{u}_w$ = wind vector
V_a = airspeed
V_g = ground point speed
V_T = track or ground speed
V_w = wind speed
V_{we} = easterly wind speed
$V_{w\text{err}}$ = error in wind speed
V_{wn} = northerly wind speed
V_ϕ = roll arc tangential velocity
v_a = V_a/V_w
v_T = V_T/V_w
α = pitch angle of sensor roll axis
β = sensor lookdown angle from the roll axis
Γ = $V_w T/H$
δ = sensor lookdown angle from the horizontal
θ = target bearing from the east axis
λ = roll arc local inclination
μ = angle defined in Fig. 1
ϕ = bank angle
ϕ_{dem} = demanded bank angle
ψ_a = aircraft heading from the east axis
ψ_{dem} = demanded heading
$\dot{\psi}_{\text{dem}}$ = demanded heading rate
$\dot{\psi}_{\text{err}}$ = heading rate error due to wind speed error
ψ_g = ground point course
ψ_T = track heading from the east axis

Special Symbols

$\bullet$ = $\mathrm{d}/\mathrm{d}t$
$'$ = $H/V_w\,\mathrm{d}/\mathrm{d}t$

Received March 27, 1997; revision received Aug. 30, 1997; accepted for publication Aug. 30, 1997.

*Senior Lecturer, Cranfield College of Aeronautics, Bedford.

Introduction

THE use of imaging sensors onboard unoccupied aircraft usually requires them to be articulated so that various regions in the vicinity of the flight path can be examined. Mounting such sensors in a dome below the aircraft provides good coverage but if the dome is fixed it imposes a significant drag penalty. Alternatively, if the dome is retractable it imposes a weight and complexity penalty. A nose-mounted sensor, on the other hand, has reduced drag but also has a smaller angular coverage. In both cases full articulation, e.g., pan and tilt, of the sensor involves complex mechanics and is further complicated by stabilization requirements. For very small aircraft (< 30 kg AUW), the weight and space penalties are important, and an obvious alternative is a strapped-down sensor on an airframe with a low angular response to gusts such as a gust-insensitive aircraft[1] configuration. Such small air vehicles generally operate at lower altitudes than larger vehicles and, hence, at shorter sight line ranges. As a result the sensor field of view used is wider, and the sight line stabilization requirements are correspondingly reduced. In a conventional bank-to-turn aircraft, however, a strapped-down sensor would only image areas on the outside of turns, and this is contrary to what is usually required. A roll-only sensor is much simpler than full articulation; it takes out the bank angle of the vehicle and enables points on either side of the flight path to be examined. It can be pointed at a specific ground point by a suitable combination of sensor roll angle and aircraft heading. The major drawback, however, is in pointing and guiding the roll-mounted sensor because the effect of wind means that the vehicle heading and the track heading are not the same. For low-speed unoccupied aircraft the airspeed can be close to the wind speed, and so the angular difference between heading and track can be very large. In that case it is not obvious that it is even possible to observe a fixed ground point from a roll-only sensor in the presence of wind.

Geometry

Without any loss of generality it can be assumed that the direction of the wind is fixed and blowing toward the north; in addition, the altitude will be assumed to be constant.

A convenient nondimensionalization scheme is given by dividing velocities by the wind speed, dividing distances by the altitude, and multiplying time by wind speed and dividing by the height. By inspection of Fig. 1, we can write

$$\sin\mu = \frac{\pm\sqrt{R^2 + H^2}\cos\delta}{R}$$

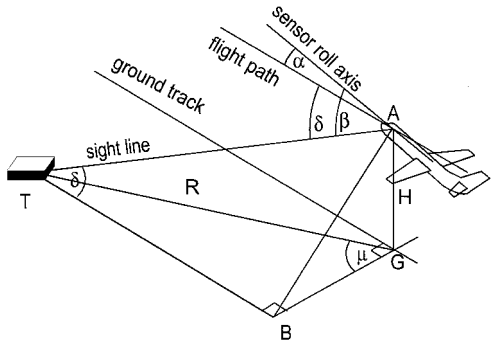

Fig. 1 Target and sensor geometry.

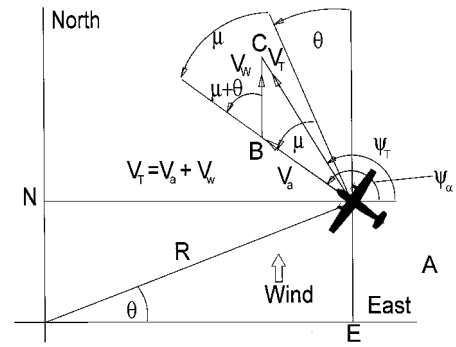

Fig. 2 Plan view of target and sensor geometry.

where the positive value is with the target to port and the negative is with the target to starboard.

The fixed lookdown angle of the sensor relative to the aircraft is β, but due to the trim angle of attack α of the roll axis, the lookdown angle relative to the horizontal is δ, given by

$$\cos\delta = \cos\alpha\cos\beta + \sin\alpha\sin\beta\cos\phi_s \tag{1}$$

where ϕ_s is the sensor roll angle. It will be assumed in what follows that the system has been designed so that α is zero. The effect of nonzero α will be considered later. In nondimensional variables we can write

$$\sin\mu = \pm\cos\delta\sqrt{1 + (1/r^2)} \tag{2}$$

This equation has some ramifications; for example, because R, H, and δ are all independent, from Eq. (2) we require

$$[1 + (1/r^2)]\cos^2\delta < 1$$

or

$$1/r < \tan\delta$$

If this condition is not satisfied, then the vehicle cannot see the ground location because δ is too small, i.e., the ground location is underneath the aircraft and the lookdown angle δ is not large enough to reach it.

For a fixed altitude and lookdown angle δ, the angle μ is just a function of range and, hence, contours of constant μ are concentric circles about the origin. If δ is $\pi/2$, then μ is constant at zero.

Kinematics

If we now consider a plan view of the situation, as shown in Fig. 2, then by inspection

$$\psi_a = \theta + \mu + (\pi/2) + (1 \mp 1)\pi \tag{3}$$

and

$$V_a = V_T\cos(\psi_a - \psi_T) - V_w\cos(\theta + \mu)$$

$$\therefore v_T\cos(\psi_a - \psi_T) = v_a \pm \cos(\theta + \mu) \tag{4}$$

Similarly,

$$\therefore v_T\sin(\psi_a - \psi_T) = \pm\sin(\theta + \mu) \tag{5}$$

Now,

$$\dot{R} = V_T\sin(\psi_a - \psi_T - \mu)$$

or using a prime to denote differentiation with respect to nondimensional time,

$$r' = v_T\sin(\psi_a - \psi_T - \mu) \tag{6}$$

Also

$$r\theta' = v_T\cos(\psi_a - \psi_T - \mu) \tag{7}$$

Expanding the range rate equation (6) gives

$$r' = \mp v_a\sin\mu + \sin\theta \tag{8}$$

Similarly for the angular rate equation (7),

$$r\theta' = \pm v_a\cos\mu + \cos\theta \tag{9}$$

Hence,

$$\frac{\mathrm{d}r}{\mathrm{d}\theta} = \frac{r(\sin\theta \mp v_a\sin\mu)}{\pm v_a\cos\mu + \cos\theta} \tag{10}$$

In Eq. (10), $\mu = \mu(r)$ and a direct integral was not obtained other than for the simpler case of $\delta = \pi/2$. However, insight into the general solution can be gained in the following way.

Let the wind speed be zero; then $v_a = \infty$ and Eq. (10) becomes

$$\frac{\mathrm{d}r}{\mathrm{d}\theta} = \mp r\tan\mu = \frac{\mp r\sqrt{r^2+1}}{\sqrt{r^2\tan^2\delta - 1}} = \text{function}(r) \tag{11}$$

because δ is fixed. Because $\mathrm{d}r/\mathrm{d}\theta$ is a single-valued monotonic function of r alone, the trajectories must be spirals that either converge to or diverge from the origin, depending on the sign of $\mathrm{d}r/\mathrm{d}\theta$, which in turn depends on the sign of $\cos\delta$. As a result, closed orbits are only possible for $\delta = \pi/2$, when $\mathrm{d}r/\mathrm{d}\theta = 0$. In addition, the trajectories are either clockwise or counterclockwise, depending on the sign of the right-hand side of Eq. (2).

Returning to the general case with $v_a \neq \infty$ and $\delta \neq \pi/2$, the track or ground speed is given by

$$v_T^2 = r'^2 + r^2\theta'^2 = 1 + v_a^2 \pm 2v_a\cos(\theta + \mu) \tag{12}$$

Using Eqs. (4) and (5),

$$\tan(\psi_a - \psi_T) = \frac{\pm\sin(\theta + \mu)}{v_a \pm \cos(\theta + \mu)} \tag{13}$$

Then, for counterclockwise spirals, using Eq. (3) results in

$$\psi_T = \theta + \mu + \tan^{-1}\left[\frac{v_a + \cos(\theta + \mu)}{\sin(\theta + \mu)}\right] \tag{14}$$

Differentiating Eq. (14) gives the yaw rate of the flight path,

$$\psi_T' = \left(1/v_T^2\right)(\theta' + \mu')\left[v_T^2 - 1 - v_a\cos(\theta + \mu)\right] \tag{15}$$

Using Eqs. (1), (2), and (8), we can obtain

$$\mu' = \frac{1}{r^2+1}\tan\mu\frac{(v_a\sin\mu - \sin\theta)}{r} \tag{16}$$

This can be substituted into Eq. (15) along with Eq. (9) to obtain the yaw rate of the flight path. Using Eqs. (3), (9), and (16) gives the heading rate

$$\psi' = \theta' + \mu' \tag{17}$$

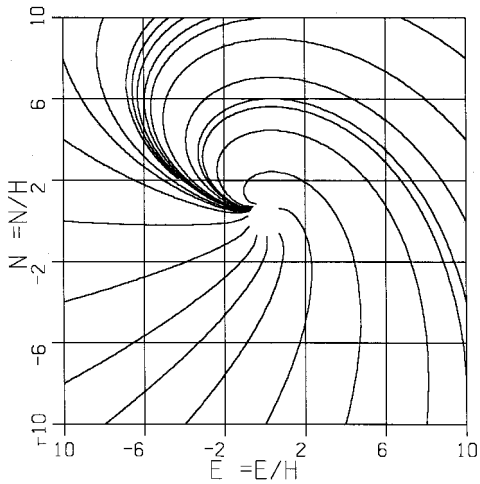

Fig. 3 Constant observation spiral trajectories in wind: V_a/V_w = 1.5, look-down = 0.7.

Numerical Solution

A numerical solution to the general case is given by solving Eqs. (1), (12), and (13) along with the following nondimensional positional equations, where the overdot denotes differentiation with respect to dimensional time:

$$\dot{e} = v_T \cos\psi_T \tag{18}$$

$$\dot{n} = v_T \sin\psi_T \tag{19}$$

$$r = \sqrt{e^2 + n^2} \tag{20}$$

$$\theta = \tan^{-1}(n/e) \tag{21}$$

A set of typical flight paths is shown in Fig. 3. For any given value of $(E/H, N/H)$, the spiral associated with that point should be followed so as to keep the ground point in view. The effect of the wind in distorting the symmetric spirals implied by the no-wind case [Eq. (11)] can be clearly seen. From any point there are two alternative trajectories, depending on whether the target is to port or to starboard. Only the counterclockwise spirals are shown in Fig. 3; the clockwise trajectories are a mirror image of the counterclockwise ones. The circle in the center represents the condition where the target is underneath the vehicle and the lookdown angle δ is no longer large enough for the target to be seen.

Orbits

As shown earlier, to orbit a ground location in the absence of wind we must have $\delta = \pi/2$. This is also the case in the presence of wind; closed orbits occur when $\delta = \pi/2$ because Eq. (10) then becomes

$$\frac{\mathrm{d}r}{\mathrm{d}\theta} = \frac{r\sin\theta}{v_a + \cos\theta} \tag{22}$$

Integration of Eq. (22) gives

$$r = \frac{1 + v_a}{v_a + \cos\theta} \tag{23}$$

If we write

$$\varepsilon = 1/v_a$$

and

$$a = v_a/(v_a - 1)$$

then Eq. (23) becomes

$$r = \frac{a(1 - \varepsilon^2)}{1 + \varepsilon\cos\theta}$$

which is the standard equation for an ellipse with eccentricity ε and semimajor axis a.

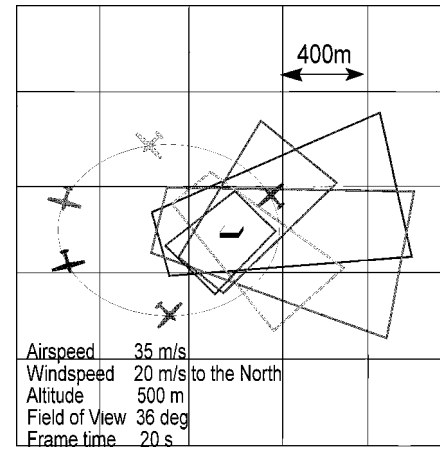

Fig. 4 Orbital trajectory and sensor footprints.

Using Eqs. (9) and (11) gives, for a constant airspeed,

$$\theta' = \frac{1 + v_a^2}{r^2} = \frac{(v_a + \cos\theta)^2}{(1 + v_a)} \tag{24}$$

and as a result we can find the nondimensional period of the orbit as

$$\Gamma = \int_0^{\Gamma} \mathrm{d}\tau = \int_0^{2\pi} \frac{(1 + v_a)\,\mathrm{d}\theta}{(v_a + \cos\theta)^2} = \frac{2\pi}{v_a}\frac{(v_a + 1)}{(v_a - 1)}\sqrt{\frac{v_a}{v_a - 1}} \tag{25}$$

The nondimensional circumference is given by

$$c = \pi\left(\frac{v_a + \sqrt{v_a^2 - 1}}{v_a + 1}\right) \tag{26}$$

The orbit shape is given by Eq. (23), and it is orientated such that the major axis is normal to the wind and the origin is one of the foci. The integration of Eq. (22) has the initial point on the positive x axis and, therefore, corresponds to the perifocus of the ellipse.

The lateral acceleration is given by Eq. (15) as

$$v_T\psi_T' = \frac{v_a(1 + v_a)^2}{v_T r^3} \tag{27}$$

This has a maximum at the perifocus given by

$$v_T\psi'_{T\max} = v_a(1 + v_a) \tag{28}$$

and as a result the maximum load factor occurs at the perifocus and is given by

$$n = \sqrt{1 + \left(V_a^2/gR_0\right)^2[1 + (V_w/V_a)]^2} \tag{29}$$

It can be seen that the wind increases the load factor for a fixed perifocus distance. The worst case would be when the wind speed equals the airspeed (orbits are not possible unless the wind speed is less than the airspeed), in which case the load factor would be almost doubled.

A typical orbital trajectory and the footprint pattern are shown in Fig. 4.

Air Vehicle Guidance

For winds blowing in an arbitrary direction, the relationship between the inertial and relative velocities is given by

$$\boldsymbol{u} = \boldsymbol{u}_r + \boldsymbol{u}_w \tag{30}$$

Consider now a new set of axes H rotated from the Earth axes E by the heading angle ψ. The direction cosine matrix (DCM) from the E axes to the H axes is $[\mathrm{DCM}]_{HE}$, and the DCM from the aircraft body axes A to the H axes is $[\mathrm{DCM}]_{HA}$. The acceleration of the vehicle in the H axes is then given by

$$\dot{\boldsymbol{u}}_H = [\dot{\mathrm{DCM}}]_{HA}\boldsymbol{u}_r + [\dot{\mathrm{DCM}}]_{HE}\boldsymbol{u}_w$$

so that

$$\dot{V}_H = -\dot{\psi}(V_{wn}\cos\psi + V_{we}\sin\psi) \tag{31}$$

In a banked turn we require

$$\tan\phi = \frac{\dot{V}_H + u\dot{\psi}}{g} = \dot{\psi}\left(\frac{u - u_w}{g}\right) = \dot{\psi}\frac{u_r}{g} \tag{32}$$

with the result that the actual heading rate is

$$\dot{\psi} = \frac{g\tan\phi}{u_r} \tag{33}$$

The demanded heading rate is then given by Eqs. (7), (12), and (17). As a result, the demanded bank angle is given by

$$\phi_{\text{dem}} = \tan^{-1}\left(\frac{\dot{\psi}_{\text{dem}}u_r}{g}\right) \tag{34}$$

The demanded heading is given from Eq. (3):

$$\psi_{\text{dem}} = \theta + \mu + (\pi/2) \tag{35}$$

The preceding equations are a simple modification to the existing flight control laws of many vehicles. Because the airspeed of the vehicle is assumed constant, an autothrottle is implied and this, in conjunction with bank angle demand, means that stall protection can be provided by limiting the bank angle.

Navigation Simulation Results

The navigation and control laws just given have been implemented in the XRAE simulation model.[2] The required additions to the simulation were estimation of the wind speed and direction (at this stage the estimates are taken to be perfect) and setting up an axis system with X in the direction of the wind, Y horizontal, and Z down. The origin of the axes is placed on the ground point to be observed. Then,

$$R = \sqrt{X^2 + Y^2} \tag{36}$$

$$\theta = \tan^{-1}(X/Y) \tag{37}$$

$$\mu = \sin^{-1}\left[\cos\delta\sqrt{1 + (H^2/R^2)}\right] \tag{38}$$

$$\psi_{\text{dem}} = -(\theta + \mu) \tag{39}$$

$$\dot{\mu} = \frac{H^2}{R^2 + H^2}\tan\mu\left(\frac{V_a\sin\mu - V_w\cos\theta}{R}\right) \tag{40}$$

$$\dot{\theta} = \frac{V_a\cos\mu + V_w\cos\theta}{R} \tag{41}$$

$$\dot{\psi}_{\text{dem}} = \dot{\theta} + \dot{\mu} \tag{42}$$

$$\phi_{\text{dem}} = K_\psi(\psi - \psi_{\text{dem}}) - \tan^{-1}\left(\frac{\dot{\psi}_{\text{dem}}V_a}{g}\right) \tag{43}$$

The rationale for these equations can be stated in the following way. Given the coordinates of the ground location and of the vehicle, plus knowledge of the wind speed and direction, then the required heading and heading rate are computed to keep the ground location in view [see Eqs. (37–42)]. Bank angle in a coordinated turn is then used to set up both the required heading and heading rate [Eq. (43)]. A typical vehicle trajectory corresponding to aircraft speed 30 m/s, height 300 m, wind speed 20 m/s, lookdown angle 1.1 rad, and field of view 36 deg and the sensor footprint are shown in Fig. 5.

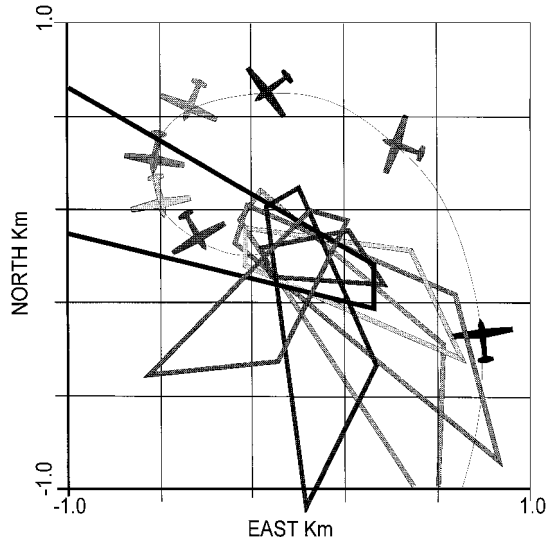

Fig. 5 Spiral approach trajectory with sensor footprints.

Influence of Errors

It was assumed that the vehicle position was measured via a tracker or a global positioning system. Errors in the positioning system will, of course, affect the trajectory but no more than for a conventionally gimballed seeker. As a result, they will not be considered further in this paper. More important are vehicle attitude errors, wind estimation errors, and height errors.

Taking the first of these, in a level coordinated turn the angle of attack of the vehicle will increase. As a result, the roll gimbal axis will no longer have the same angle to the horizontal. This will generate an error in the previously assumed geometry. However, it can be either measured or calculated for a specific vehicle type and flight condition because it is a function of speed and the bank angle. It can be accommodated in the guidance calculations as a modification of the δ angle. If α is small, then from Eq. (1) we can approximate it as

$$\delta = \beta - \alpha\cos\phi_s$$

Errors caused by wind estimation have two components. The first is the effect of the magnitude of the wind velocity on the heading rate, i.e.,

$$\dot{\psi}_{\text{err}} = \frac{V_{w\text{err}}}{R}\left(\cos\theta - \frac{H^2}{H^2 + R^2}\tan\mu\sin\theta\right)$$

from Eqs. (40–42). This rate is inversely proportional to range and has only a minor effect on the aircraft trajectory (compare Figs. 5 and 6).

The second error component is in wind direction as this translates directly into an equivalent error in the aircraft heading. That this is the more important source of error can be inferred from comparing Figs. 5 and 7.

To point the sensor at the target, the vertical separation between the aircraft and the target is required. This, of course, might be in error due to altimeter errors or terrain topography. Walster[3] has shown that such errors result in the target image having a motion relative to the bore sight such that a couple of cursor fixes by the operator of the target position on the screen relative to the boresight enables a correction to be obtained for the height error. In this way height-above-grounderrors are easily removed.

Linear Search

The preceding analysis has concentrated on point observation, but it is useful to ask whether the ground observation point can have a prescribed velocity so that a linear search can be undertaken. The bore sight ground intersection can have a velocity owing to the aircraft's track velocity or ground speed, the aircraft's rate of change of heading, and the roll rate of the sensor.

The first of these has the same magnitude and direction as the aircraft's ground speed, whereas the second is normal to the ground

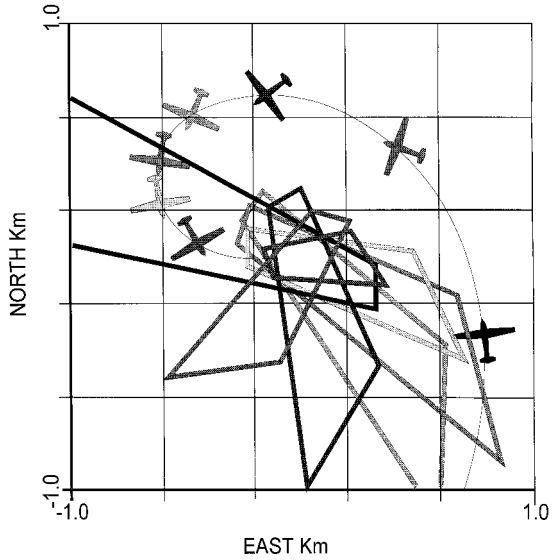

Fig. 6 Effect of a 5-m/s wind estimate error on the trajectory and the sensor footprints.

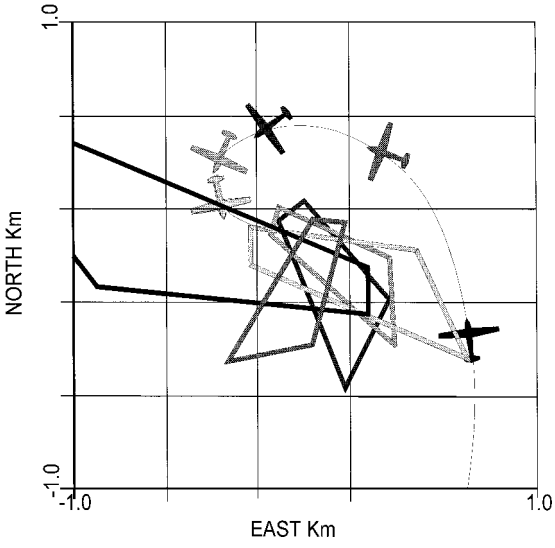

Fig. 7 Effect of a 0.1-rad wind bearing estimation error on the trajectory and the sensor footprints.

radius vector. The third is tangential to the roll arc, that is, the hyperbola that results from the intersection of the ground plane and the cone generated by rolling the bore sight. Because by a suitable choice of roll rate, any velocity required tangential to the roll arc can be generated, we only need to consider initially the components of the first two normal to the roll arc.

The coordinates of the ground point in Fig. 8 are given by

$$X = R\cos\mu, \qquad Y = R\sin\mu \tag{44}$$

and converting to nondimensional form and using Eqs. (1) and (2) gives the equation of the roll arc as

$$y^2\tan^2\delta - x^2 = 1 \tag{45}$$

This is the equation of a hyperbola with asymptotes given by

$$x/y = \pm\tan\delta$$

The slope of the roll arc is given by

$$\frac{\mathrm{d}y}{\mathrm{d}x} = \frac{x}{y}\frac{1}{\tan^2\delta} = \frac{1}{\tan\mu}\frac{1}{\tan^2\delta} = \tan\lambda \tag{46}$$

Let the angle between the local tangent to the roll arc and the radius vector be

$$\gamma = \mu - \lambda \tag{47}$$

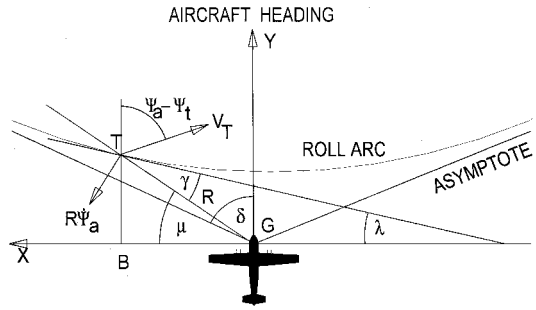

Fig. 8 Geometry definitions for the linear search case.

Referring to Fig. 8 we can compute the normal and tangential components of V_T normal to and along the local tangent to be, respectively,

$$V_T\sin[\gamma + (\pi/2) - \mu + \psi_a - \psi_T] \tag{48}$$

$$V_T\cos[\gamma + (\pi/2) - \mu + \psi_a - \psi_T] \tag{49}$$

whereas the normal and tangential components, respectively, of $R\dot{\psi}_a$ are

$$-R\sin[\pi - \mu - (\pi/2) + \mu - \gamma] \tag{50}$$

$$R\cos[\pi - \mu - (\pi/2) + \mu - \gamma] \tag{51}$$

Let the track and speed of the ground point be ψ_g and V_g, respectively. Then resolving as before gives the normal and tangential components, respectively,

$$V_g\sin(\pi - \psi_g - \lambda) \tag{52}$$

$$V_g\cos(\pi - \psi_g - \lambda) \tag{53}$$

Summing the normal components to zero, we can solve for $\dot{\psi}_a$ and obtain

$$\dot{\psi}_a = \frac{-V_g\sin(\psi_g + \lambda) + V_T\cos(\gamma - \mu + \psi_a - \psi_T)}{R\cos\gamma} \tag{54}$$

Expanding the cosine term and using Eqs. (6) and (7) yields

$$\dot{\psi}_a = \frac{-V_g\sin(\psi_g + \lambda)}{R\cos\gamma} + \dot{\theta} - \tan\gamma\frac{\dot{R}}{R} \tag{55}$$

Using Eq. (47) along with Eqs. (1) and (2), we can show

$$\tan\gamma = \tan\mu/(r^2 + 1) \tag{56}$$

and using this with Eqs. (8) and (16) gives

$$\dot{\psi}_a = \frac{-V_g\sin(\psi_g + \lambda)}{R\cos\gamma} + \dot{\theta} + \dot{\mu} \tag{57}$$

and for zero ground point speed this reverts to Eq. (42). If we denote the tangential velocity of the ground point along the roll arc as V_ϕ, then we can sum the tangential components to give

$$V_\phi = R\sin(\dot{\theta} - \dot{\psi}_a) - \frac{R^2 + H^2}{H^2}\frac{R\dot{\mu}\cos\gamma}{\tan\mu} - V_g\cos(\psi_g + \lambda) \tag{58}$$

The required roll rate of the sensor can then be found as follows:

$$x = \tan\phi_s, \qquad \dot{x} = \frac{-\dot{\phi}_s}{\cos^2\phi_s}$$

Using Eq. (46),

$$\dot{\phi}_s = \frac{V_\phi\cos^2\phi_s\cos\lambda}{H} \tag{59}$$

The required sensor roll angle is given by

$$\phi_s = \frac{R\cos(\mu)}{H} \tag{60}$$

These equations provide the guidance laws for a moving ground point. The heading and heading rate controls are essentially the same as before but with Eq. (57) in place of Eq. (42). The sensor roll angle is unchanged, but a roll rate demand is now included.

For linear search with a 90-deg lookdown angle, the closed orbits associated with point observation become cycloids. The preceding linear search algorithm also allows area search using a zigzag linear search pattern.

Conclusions

It has been shown that a roll-only sensor can be used for point, line, and area ground observation in wind provided that the aircraft is flown on the correct trajectory. The trajectories have been derived and depend on the lookdown angle, the airspeed of the vehicle, and the magnitude and direction of the wind speed. If the lookdown angle is 90-deg, then for point observation the trajectories become elliptical orbits with the target at one of the foci. Flight guidance laws have also been derived and demonstrated on a six-degree-of-freedom simulation. They use bank angle to generate the required heading and heading rate. Point, line, and area search capabilities have also been demonstrated. The effect of trim angle and wind estimation errors have been considered and illustrated, and the estimation of wind direction is seen to be an important parameter. In conclusion, the use of a roll-only sensor provides the opportunity to reduce the weight, drag, and mechanical complexity of the sensor installation and replace them with guidance software. The guidance algorithms uncouple the operator's involvement in flight control and sensor control, so that the operator can just fly the footprint of the sensor and leave the guidance of the vehicle to the flight control system, thereby significantly simplifying the operator function.

Acknowledgment

The work described was supported by the Ministry of Defense (Operational Requirements), Artillery and Air Defense.

References

[1]Thomasson, P. G., "The Flight Dynamics of an Unstable Unmanned Aircraft," *Aerospace Vehicle Dynamics and Control*, edited by M. V. Cook and M. J. Ryecroft, Clarendon, Oxford, England, UK, 1994, pp. 245–258.

[2]Thomasson, P. G., "The Use of Simulation in the Development of a Gust Insensitive Aircraft," Proceedings of the United Kingdom Simulation Council Conf. on Computer Simulation, Brighton, England, UK, Sept. 1990.

[3]Walster, R. A., "Try It Before You Fly It," Proceedings of the 12th Bristol International Remotely Piloted Vehicles Conf., Bristol, England, UK, Sept. 1996.